The International Journal of Advanced Manufacturing Technology (2018) 96:4333–4343
https://doi.org/10.1007/s00170-018-1893-1

ORIGINAL ARTICLE

Coupling stress caused by thermal and slicing force in KDP crystal slicing with fixed abrasive wire saw

Zongqiang Li[1] · Peiqi Ge[1,2] · Wenbo Bi[1] · Tengyun Liu[1] · Peizhi Wang[1] · Yufei Gao[1]

Received: 29 September 2017 / Accepted: 13 March 2018 / Published online: 23 March 2018

Abstract

KDP (KH_2PO_4) crystal is an important functional crystalline material that can be used in the area of laser frequency conversion. As the first process of machining, the slicing process of the KDP crystal is of vital importance to the yield rate of wafers. While the KDP crystal often cracks in the slicing process by the traditional method of band saw because of its properties of high brittleness, low strength, and high thermal sensitivity, the cracks may lead to waste of the whole KDP crystal and should be avoided. Fixed abrasive wire saw slicing is considered a preferred method for KDP crystal slicing due to its advantage of low sling stress. In this paper, a finite element model in fixed abrasive wire saw slicing of the KDP crystal is established with respect to distributed slicing force and thermal stress. Distribution of slicing force and heat around the kerf area is deduced and applied to the finite element model. Based on the model, temperature field and stress field of the KDP crystal in the slicing process is obtained. The maximum principle stress caused by slicing force, thermal stress, and coupling of the slicing force and thermal stress is obtained. The maximum principle stress of different slicing parameters is analyzed; function equation between the maximum principle stress and slicing parameter is obtained by the least squares method. The critical slicing parameter at which cracks would not occur in the slicing is obtained. The simulation results in this paper are useful to avoid cracking in KDP crystal slicing with fixed abrasive wire saw.

Keywords KDP crystal · Fixed abrasive wire saw · Temperature field · Coupling stress of slicing force and thermal stress

Nomenclature

c	Specific heat of the KDP crystal
F_{gn}	Normal force of single abrasive grit
F_{gt}	Tangential force of single abrasive grit
F_n	Total normal force applied by the wire saw
$F_{n\theta}$	Distributed normal force applied by the wire saw
F_t	Total tangential force applied by the wire saw
$F_{t\theta}$	Distributed normal force applied by the wire saw
K	Ratio of chip deforming force to the normal force
k_1	Heat conductivity coefficient in [001] crystal orientation of the KDP crystal
k_2	Heat conductivity coefficient in [010] and [100] crystal orientation of the KDP crystal
l	Contact length between the wire saw and the KDP crystal
m	Number of abrasive in unit area
P	Power of heat absorbed by the KDP crystal in slicing
P_θ	Distributed heat power in kerf area
r	Radius of the wire saw
S	Compliance matrix of the KDP crystal
s_{ij}	Compliance constant of the KDP crystal
$S_{\max}$	Maximum principle stress in the KDP crystal
v_s	Wire saw speed.
v_w	Feed speed of the KDP crystal
α_1	Coefficient of thermal expansion in [010] and [100] crystal orientation of the KDP crystal
α_2	Coefficient of thermal expansion in [001] crystal orientation of the KDP crystal
β	Half conical angle of the abrasive
ε	Strain matrix of the KDP crystal
ε_{ij}	Strain component

✉ Peiqi Ge
pqge@sdu.edu.cn

[1] School of Mechanical Engineering, Shandong University, Jinan 250061, China

[2] Key Laboratory of High-Efficiency and Clean Mechanical Manufacture at Shandong University, Ministry of Education, Jinan 250061, China

η	Heat absorption rate of the KDP crystal
λ	Ratio of the abrasives participated in the slicing
θ	Location angle of abrasive in the section of wire saw
ρ	Density of KDP crystal
$\boldsymbol{\sigma}$	Stress matrix
σ_{c1}	Compressive strength in [001] crystal orientation
σ_{c2}	Compressive strength in [010] and [100] crystal orientation
σ_{t1}	Tensile strength in [001] crystal orientation of the KDP crystal
σ_{t2}	Tensile strength in [010] and [100] crystal orientation of the KDP crystal
σ_{ij}	Stress component
σ_{sy}	Average contact pressure between abrasives and the KDP crystal

1 Introduction

KDP (KH_2PO_4, potassium dihydrogen phosphate) crystal is an important functional crystalline material widely used in the area of laser frequency conversion and electro-optical modulation because of its properties of large laser damage threshold, large electro-optic, and nonlinear optical coefficient [1–3]. As KDP can grow to a large-scale crystal, it is the only material that can be used in inertial confinement fusion technology.

Most studies of the KDP crystal focused on the ultra-precision machining of the KDP crystal mainly. Chen N [4] achieved ductile cutting of the KDP crystal using the micro-polycrystalline diamond ball end milling. Zong WJ [5] carried out diamond fly cutting experiments of the KDP crystal and investigated the influence of tool geometries to the surface topography. To achieve crack-free and high-efficiency ultra-precision machining of the KDP crystal, Chen D [6] proposed a hybrid machining method by combining precision grinding with fly cutting. The experimental results showed that the machining efficiency of the hybrid method is five times to that of the cutting process. Wang X [7] developed a new method of machining the KDP crystal based on the solubility of the KDP crystal in water. The method was proved able to remove the micro-waviness and subsurface damage of the KDP crystal.

The KDP crystal should be sliced into pieces before the ultra-precision machining. As the first process of obtaining wafers, slicing is of vital importance to the follow-up processes and production of wafers. The slicing process determines the utilization rate of the KDP crystal and processing allowance of the following processes.

The KDP crystal is easy to crack in the processes of growing, machining, and even transferring because of its properties of high brittleness, low strength, and high thermal sensitivity [8–10]. In the process of slicing, cracks may lead to the waste of the whole KDP crystal. While in the slicing of other material such as silicon and silicon carbide, cracks may not lead to the waste of the whole crystal due to their stronger material mechanical properties. That is to say, cracks in the slicing of the KDP crystal is a serious and unique problem that should be studied.

Free abrasive wire saw cannot be used in the slicing of the KDP crystal. As the hardness of the KDP crystal is low, free abrasives may get stuck into the KDP crystal by the method of free abrasive wire saw. Band saw is a customary method of slicing the KDP crystal. But cracks often occur and lead to the waste of the whole crystal as the KDP crystal may suffer a large slicing force because of the twist of band.

Compared to free abrasive wire saw, abrasives in fixed abrasive wire saw can easily reach the machining region as they are fixed to the wire saw [11, 12]. Schematic of KDP crystal slicing with fixed abrasive wire saw is illustrated in Fig. 1. Compared to band saw, the fixed abrasive wire saw applies a smaller force to the KDP crystal because of the flexibility of the wire saw. Many studies have been done about fixed abrasive wire saw but mainly focused on silicon carbide, silicon, and ceramics [13–15]. Preliminary experimental research on the KDP crystal slicing with fixed abrasive wire saw has been done by orthogonal tests [16]. And optimized slicing parameter combination considering the surface morphology and surface roughness is obtained. As fixed abrasive wire saw has advantages of low slicing stress and the ability to slicing large-scale crystal [17, 18], it is a preferred method of KDP slicing and expected to solve the problem of cracking in the slicing of the KDP crystal.

The KDP crystal would crack when the stress exceed its tensile strength in the slicing process. Thermal stress and slicing force applied by the wire saw are two main aspects of the stress in the slicing. To investigate the influence of slicing parameters to cracking, thermal stress, and stress field of the crystal in fixed abrasive wire saw slicing process should be

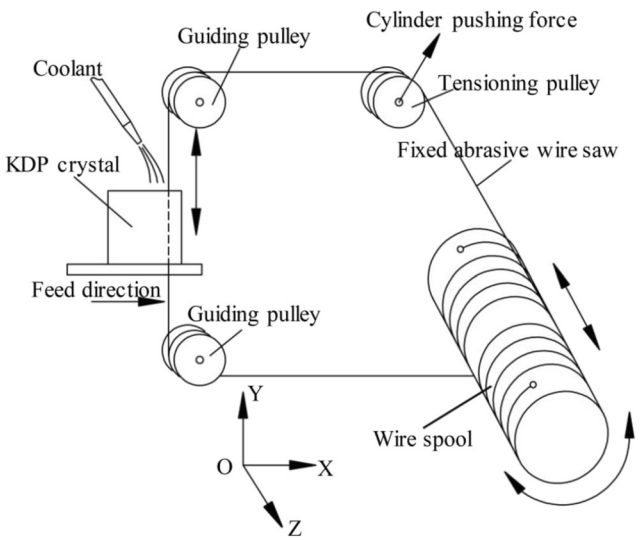

Fig. 1 Schematic of the KDP crystal slicing with fixed abrasive wire saw

studied. Zhang Q and Zhang N [19, 20] simulated the internal stress of KDP in the processes of crystal growing and taken out from the crystal growth slot and found that the stress of the KDP crystal is affected by its crystal size. Ge M [21] simulated the stress in the KDP crystal caused by slicing force in fixed abrasive wire saw slicing. It is considered that the stress is very small in the KDP crystal while the thermal stress is not considered. As the high thermal sensitivity of the KDP crystal, the influence of thermal stress should not be ignored.

Temperature change in the wire saw slicing has been studied by some researchers. Bhagavat S [22] constructed a finite element model and analyzed the temperature variation of silicon in free abrasive wire saw slicing. Johnsen L [23] studied the temperature field of silicon in free abrasive wire saw slicing and thought that the viscous dissipation is the main source of heat. Jiao Y [24] simulated the temperature of the KDP crystal in fixed abrasive wire saw slicing and got the thermal stress on the kerf. Though the temperature change in wire saw slicing has been studied by some researchers, the influence of slicing parameters to the slicing stress has not been studied while the influence of slicing parameters to thermal stress and coupling of slicing stress and thermal stress should be further studied.

As temperature stress and slicing force applied by the wire saw are two main parts of slicing stress, temperature field and stress field of the KDP crystal in fixed abrasive wire saw slicing is simulated in this paper. In order to obtain the critical slicing parameters at which cracks would not occur in the slicing of the KDP crystal, influence of slicing parameters to the temperature field and the stress field of the KDP crystal is simulated by the established model. The results may provide a theoretical basis to avoid cracking in the KDP crystal slicing with fixed abrasive wire saw.

2 Analysis of slicing force

In fixed abrasive wire saw slicing, analysis of slicing force for silicon carbide [12] and silicon [25] has been studied. But the slicing force analysis for the KDP crystal by fixed abrasive wire saw is not reported. The schematic of force applied by wire saw to the KDP crystal in the view of the cross section of the wire saw is illustrated as Fig. 2. The coordinate system corresponds with the global system. The force applied to the KDP crystal by wire saw in the slicing process can be separated into the normal force F_n and the tangential force F_t. F_n is vertical to the contact surface in the direction of –X while F_t is consistent with the move direction of wire saw in the direction of –Y.

It can be seen from Fig. 2 that there are abrasives on the surface of the wire saw. The angle θ indicates the position of the abrasives on the wire saw. In Fig. 2, v_w is the feed speed of the KDP crystal in the direction of X, v_s is the wire saw speed

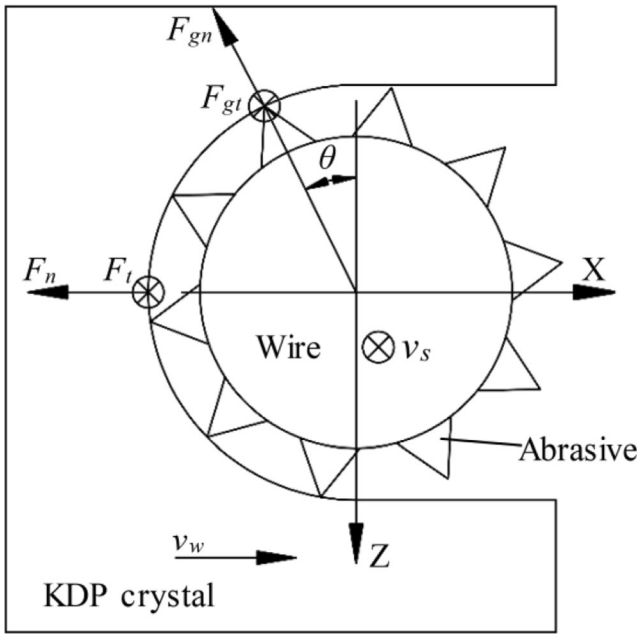

Fig. 2 Schematic of force on the cross section of wire saw

in the direction of -Y. F_{gn} is the normal force of single abrasive grit whose direction is vertical to the kerf surface. F_{gt} is the tangential force of single abrasive grit whose direction is parallel to the wire saw axis.

Abrasives are assumed evenly distributed on the surface of fixed abrasive wire saw. The abrasives are in the shape of conical. The location angle of the abrasive in the section of wire saw is defined as θ. It can be noticed from Fig. 2 that only half of the abrasives contract with the KDP crystal in the slicing. So the angle θ is in the range of 0 to π. The slicing force of single abrasive is derived as Eq. (1) [26]:

$$\begin{cases} F_{gn} = \left(\dfrac{2K}{m} + \dfrac{\pi\sigma_{sy}\tan\beta}{2m}\right)\dfrac{v_w \sin\theta}{v_s} \\ F_{gt} = \left(\dfrac{K\pi}{2} + \dfrac{\pi\mu\sigma_{sy}\tan^2\beta}{2}\right)\dfrac{1}{m\tan\beta}\dfrac{v_w \sin\theta}{v_s} \end{cases} \tag{1}$$

In Eq. (1), K is the ratio of chip deforming force to the normal force. β is the half conical angle of abrasive. σ_{sy} is the average contact pressure between abrasives and the KDP crystal, it is a constant value in this study while m is the number of abrasive in unit area on the surface of wire saw. The parameters in Eq. (1) can be instead by A and B as Eq. (2):

$$\begin{cases} A = \dfrac{2K}{m} + \dfrac{\pi\sigma_{sy}\tan\beta}{2m} \\ B = \left(\dfrac{K\pi}{2} + \dfrac{\pi\mu\sigma_{sy}\tan^2\beta}{2}\right)\dfrac{1}{m\tan\beta} \end{cases} \tag{2}$$

As all the parameters on the right side of Eq. (2) are determined by the material properties and the condition of wire saw in the slicing, they are constant values in this study. So A and B

can be considered unchanged in the study. Then, Eq. (1) can be rewritten to the following forms:

$$\begin{cases} F_{gn} = A\dfrac{v_w \sin\theta}{v_s} \\ F_{gt} = B\dfrac{v_w \sin\theta}{v_s} \end{cases} \tag{3}$$

The expression of total normal force F_n and the total tangential force F_t can be acquired as Eq. (4) by calculating slicing force of all the abrasives according to Eq. (1). Where l is the contact length between the wire saw and the KDP crystal whose value is 20 mm, r is the radius of the wire saw with the value of 0.2 mm. While λ is the ratio of the abrasives participated in the slicing, it can be considered unchanged in the study:

$$\begin{cases} F_n = A\dfrac{\pi mlr\lambda}{2}\dfrac{v_w}{v_s} \\ F_t = 2Bmlr\lambda\dfrac{v_w}{v_s} \end{cases} \tag{4}$$

The relationship between the total slicing force and the force of single abrasive can be acquired as Eq. (5) according to Eqs. (1) and (4):

$$\begin{cases} F_{gn} = \dfrac{2\sin\theta}{\pi mlr\lambda}F_n \\ F_{gt} = \dfrac{\sin\theta}{2mlr\lambda}F_t \end{cases} \tag{5}$$

Compute the integral of Eq. (1) while θ is in the range of 0 to π and combine it with Eq. (4) and Eq. (5). The distribution of slicing force can be obtained as Eq. (6) which can be exerted to the simulation model:

$$\begin{cases} F_{n\theta} = Am\lambda\dfrac{v_w}{v_s}\sin\theta \\ F_{t\theta} = Bm\lambda\dfrac{v_w}{v_s}\sin\theta \end{cases} \tag{6}$$

where $F_{n\theta}$ is the distributed normal force applied by the wire saw to the crystal whose direction is vertical to the kerf. $F_{t\theta}$ is the distributed tangential force applied by the wire saw whose direction is consistent with the moving direction of the wire saw. Schematic of their amplitude is shown in Fig. 3.

The power of heat absorbed by the KDP crystal in the slicing can be obtained as the following forms:

$$P = \eta F_t v_s \tag{7}$$

where η is the heat absorption rate of the KDP crystal whose value is 1/3 [22]. As the tangential force is distributed load in the kerf as shown in Eq. (6), the distribution of the heat power can be derived as Eq. (8):

$$P_\theta = \eta Bm\lambda v_w \sin\theta \tag{8}$$

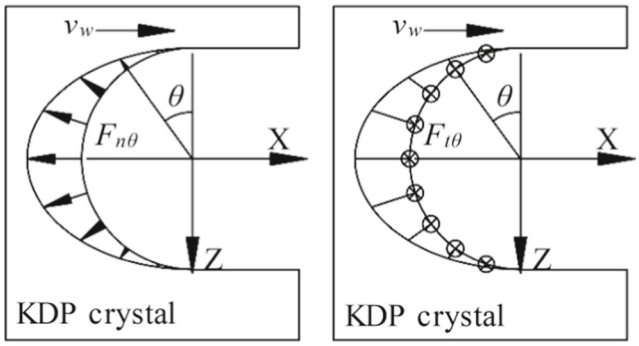

(a) $F_{n\theta}$ (b) $F_{t\theta}$

Fig. 3 Schematic of the amplitude of the distributed slicing force $F_{n\theta}$ and $F_{t\theta}$ on the wire saw section

where P_θ is the distributed heat power in the kerf area. As the parameters $\eta Bm\lambda$ are constant values in the simulation, so the power only changes with the feed speed of the KDP crystal v_w in this condition. The distribution of heat power in the section of wire saw is shown in Fig. 4.

When the wire saw speed v_s is 1.5 m/s and the feed speed v_w is 0.6 mm/min, the normal slicing force F_n is 3.2 N and the tangential force F_t is 1.6 N, respectively. The normal force is got by the tension force in the wire saw and the bend of the wire saw. Put the parameters into Eq. (6) and Eq. (8), then the values of the force applied to the finite element model can be acquired as Eq. (9):

$$\begin{cases} F_{n\theta} = \dfrac{2\cos\theta}{\pi lr}F_n = Am\lambda\dfrac{v_w}{v_s}\cos\theta \\ F_{t\theta} = \dfrac{\cos\theta}{2lr}F_t = Bm\lambda\dfrac{v_w}{v_s}\cos\theta \\ P_\theta = \eta\dfrac{F_t v_s}{2lr}\cos\theta == \eta Bm\lambda v_w\cos\theta \end{cases} \tag{9}$$

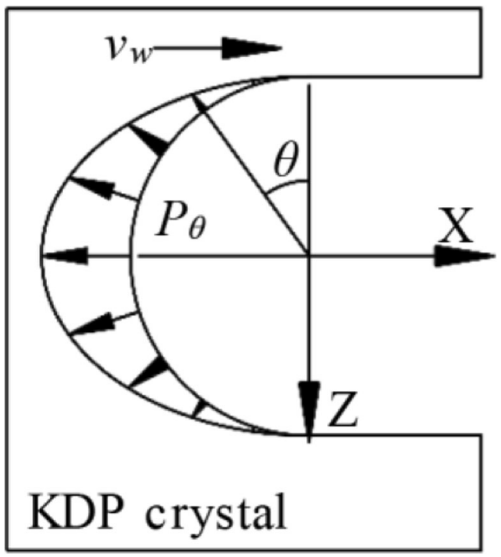

Fig. 4 Schematic of the distributed heat power in the wire saw section

as the parameters A, B, m, λ can be considered unchanged in this model as mentioned above. It can be seen from Eq. (9) that $F_{n\theta}$ and $F_{t\theta}$ only changes with the value of v_w/v_s while P_θ only changes with v_w.

When slicing parameters changes, the force and heat power applied to the model would also change according to Eq. (9). In this way, the slicing process of different parameters can be simulated. Different groups of slicing parameters are chosen to investigate the influence rule of slicing parameters to the maximum principle stress of the KDP crystal.

3 Model of simulation and material parameters

3.1 Model of simulation

Based on the mechanism of fixed abrasive wire saw, a finite element model is built to simulate the slicing process of the KDP crystal by fixed abrasive wire saw. The wire saw is instead by the force applied by the wire saw to simplify the model. Some other assumptions are also made. The residual stress of the KDP crystal is supposed released before the slicing. As the wire saw and the KDP crystal contact with a length in the slicing process, the vibration of the wire saw is restricted by the KDP crystal. The influence of vibration is little and ignored in the model. In the slicing, the wire saw would bend in a small angle because of the feeds of the KDP crystal. The processing track is considered straight line to simplify the model.

The geometric model of the KDP crystal in the simulation and its coordinate system is shown in Fig. 5a. The KDP crystal in the simulation is cuboid in shape with the dimension of $20 \times 20 \times 40$ mm while the width of the kerf is 0.4 mm. The KDP crystal feeds in the X direction while the wire saw moves in the Y direction. In other words, the crystal is sliced in the (001) crystal plane, the KDP crystal feeds in [100] crystal orientation while the wire saw moves in [010] crystal orientation.

The element type used in the model is C3D8I. Meshes around the kerf are refined to increase the accuracy of the simulation; it is the dark area shown in Fig. 5b. Grid-independence verification of the FEM model is conducted. Simulation results of the model with different number of meshes are compared. At last, the model is chosen which has 59,493 elements and 62,628 nodes, respectively.

Removal of material is simulated by the birth and death algorithm. The slicing process is divided to many steps. Also, material of the slicing kerf is also divided into many parts. In every step of the simulation, one part of the slicing kerf is removed; the node force of the elements after slicing are settled to zero by the birth and death algorithm and not included in the subsequent steps. At the same time, stress and heat power are applied to the newly formed kerf area. Then, the slicing process can be simulated.

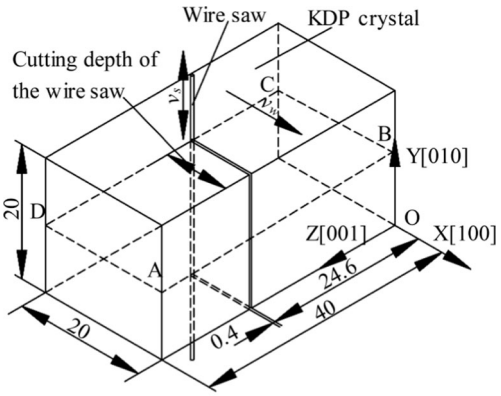

(a) Geometric model of KDP crystal

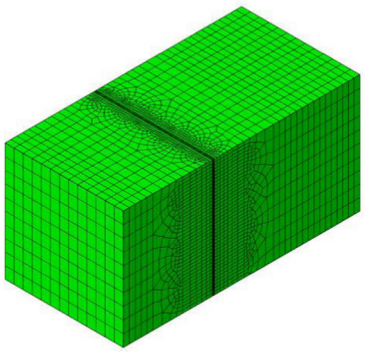

(b) Finite model of the KDP crystal

Fig. 5 Geometric and finite model of the KDP crystal. **a** Geometric model of the KDP crystal. **b** Finite model of the KDP crystal

3.2 Material parameters applied to the finite element model

As the KDP crystal is in a tetragonal phase at room temperature, it is a kind of typical anisotropic elastic-brittle material with the material parameters shown in Table 1.

As shown in Fig. 6, the natural habit of the KDP crystal grown from solution is a tetragonal prism combined with a tetragonal bipyramid. Its prism faces are (100) and (010) planes while [001] is the prism axis.

The stress-strain expression of the KDP crystal is Eq. (10):

$$\varepsilon = \begin{Bmatrix} \varepsilon_{11} \\ \varepsilon_{22} \\ \varepsilon_{33} \\ \gamma_{13} \\ \gamma_{23} \\ \gamma_{12} \end{Bmatrix} = \begin{bmatrix} s_{11} & s_{12} & s_{13} & 0 & 0 & 0 \\ s_{12} & s_{11} & s_{13} & 0 & 0 & 0 \\ s_{13} & s_{13} & s_{33} & 0 & 0 & 0 \\ 0 & 0 & 0 & s_{44} & 0 & 0 \\ 0 & 0 & 0 & 0 & s_{44} & 0 \\ 0 & 0 & 0 & 0 & 0 & s_{66} \end{bmatrix} \begin{Bmatrix} \sigma_{11} \\ \sigma_{22} \\ \sigma_{33} \\ \sigma_{13} \\ \sigma_{23} \\ \sigma_{12} \end{Bmatrix} = \boldsymbol{S}\boldsymbol{\sigma} \quad (10)$$

where ε is the strain matrix, $\boldsymbol{S}$ is the compliance matrix, $\boldsymbol{\sigma}$ is the stress matrix, ε_{ij} is strain component, s_{ij} is compliance

Table 1 Material parameters of the KDP crystal [27–29]

Parameters	Value
Coefficient of thermal expansion in [010] and [100] crystal orientation α_1/(K^{-1})	2.454×10^{-5}
Coefficient of thermal expansion [001] crystal orientation α_2/(K^{-1})	4.168×10^{-5}
Compressive strength in [001] crystal orientation σ_{c1}/(MPa)	115.00
Compressive strength in [010] and [100] crystal orientation σ_{c2}/(MPa)	93.2
Density ρ/(kg•m^{-3})	2338
Heat conductivity coefficient in [001] crystal orientation k_1/(W/(m•°C))	1.34
Heat conductivity coefficient in [010] and [100] crystal orientation k_2/(W/(m•°C))	1.21
Specific heat c/(J/(kg•°C))	857
Tensile strength in [001] crystal orientation σ_{t1}/(MPa)	8.35
Tensile strength in [010] and [100] crystal orientation σ_{t2}/(MPa)	6.67

coefficient, and σ_{ij} is stress component. All the mechanical properties of the KDP crystal in the simulation model can be defined by the compliance matrix $\boldsymbol{S}$.

Compliance coefficients of the KDP crystal are shown in Table 2. According to the compliance coefficients and Eq. (10), all the mechanical properties can be defined in ABAQUS. The stiffness matrix then can be got by the compliance matrix $\boldsymbol{S}$ and applied to ABAQUS as the mechanical properties.

4 Results and discussion

Because of the brittle property of the KDP crystal, the KDP crystal is easy to crack due to tensile stress. It can be seen from Table 1 that the tensile strength of the KDP crystal is much smaller than the compressive strength. The tensile strength of the KDP crystal is chosen as the criteria of cracking. Tensile stress of the KDP crystal is chosen and compared to the tensile strength to study the cracking of the KDP crystal [8, 9, 19, 20]. So in this study, the major principal stress theory is used to evaluate whether the crystal would crack.

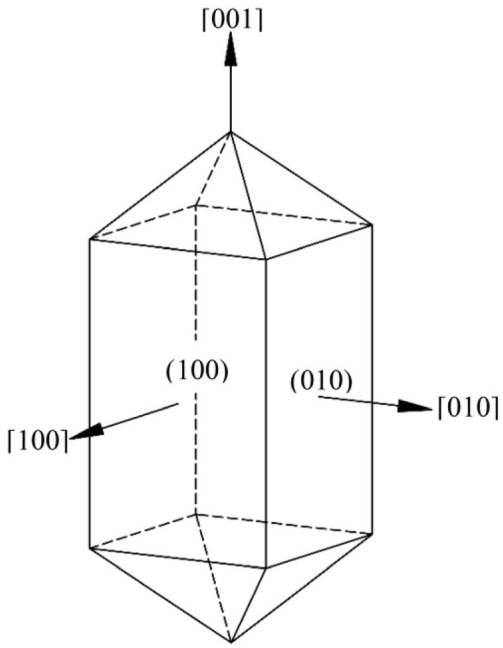

Fig. 6 Crystal structure of the KDP crystal

4.1 Maximum principle stress caused by slicing force

While the cutting depth of wire saw is 10 mm, the wire saw speed v_s is 1.5 m/s and the feed speed v_w is 0.6 mm/min, distribution of maximum principle stress caused by slicing force in the KDP crystal is shown in Fig. 7. It can be seen that the maximum principle locates in the outlet of the kerf area. When there is only slicing stress, the maximum principle stress of the KDP crystal in the slicing is about 0.063 MPa, which is much smaller than the strength of the KDP crystal.

The outlet of kerf is often the place where the edge breakage occurs but not the crack of the whole crystal. Cracks often appear in the middle plane of the KDP crystal in the slicing. To study the maximum principle stress in slicing and influence of slicing parameters to the maximum principle stress, the maximum principle stress in plane ABCD is chosen as the object in this study.

Distribution of maximum principle stress caused by slicing force in plane ABCD is shown in Fig. 8. It can be seen that the maximum principle stress around the kerf area is small because of the press of wire saw while the maximum principle stress around the places behind the kerf is large because of the pull of the wire saw.

The variation of the maximum principle in plane ABCD is shown in Fig. 9. It can be seen that the maximum principle stress increases rapidly to about 5×10^{-4} MPa in the

Table 2 Compliance coefficients of the KDP crystal [30]

Compliance constant	s_{11}	s_{12}	s_{13}	s_{33}	s_{44}	s_{66}
Value (GPa^{-1})	0.0151	0.0018	−0.004	0.0195	0.0751	0.162

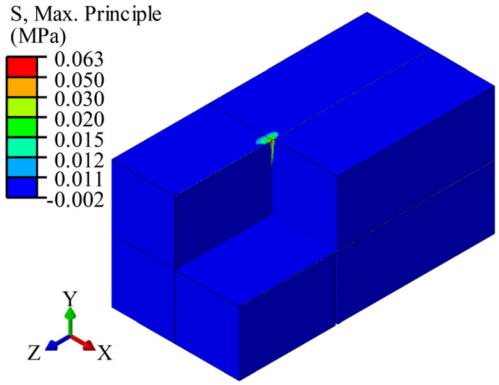

Fig. 7 Distribution of maximum principle stress caused by slicing force

beginning stage of the slicing. The stress keeps increasing in the middle stage of the slicing process. While in the end of slicing, the stress reaches the largest value of about 22.5×10^{-4} MPa because of the stress concentration. It can be noticed that the maximum principle stress in the slicing is much less than the tensile strength of the KDP crystal. This can be understood that the wire saw slicing is a method of the low stress slicing method.

4.2 Maximum principle stress caused by thermal stress

4.2.1 Temperature field in the slicing

While the cutting depth of wire saw is 10 mm, the wire saw speed v_s is 1.5 m/s and the feed speed v_w is 0.6 mm/min; distribution of temperature field in the slicing is shown in Fig. 10. Temperature of the KDP crystal rises because of the heat generated by the slicing force. It can be seen that the maximum temperature locates in the kerf area. The closer to the kerf, the higher is the temperature. The temperature drops after the wire saw leaves.

It can be seen from Fig. 11 that the maximum temperature of the KDP crystal almost remains stable in the slicing. There

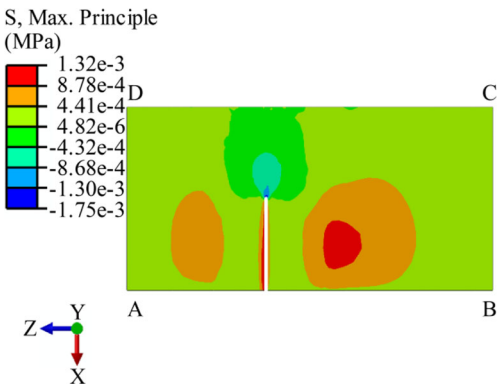

Fig. 8 Maximum principle stress caused by slicing stress in plane ABCD

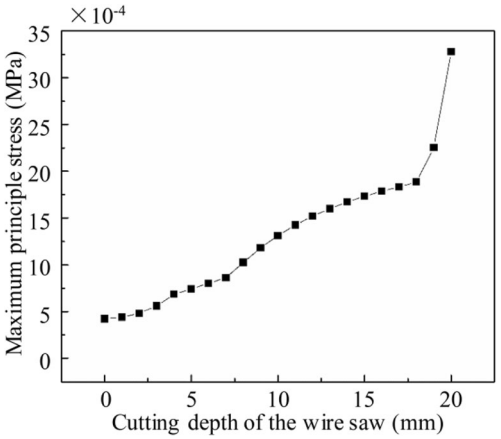

Fig. 9 Variation of the maximum principle stress caused by slicing stress in plane ABCD

is no rapid change in temperature after heat balance is achieved in the slicing.

4.2.2 Maximum principle stress caused by thermal stress in plane ABCD

The distribution of maximum principle stress caused by thermal stress in plane ABCD is shown in Fig. 12. It can be seen from Fig. 12 that the maximum principle stress occurs around the newly formed kerf behind the slicing area, but not in the slicing place where the temperature is the highest.

The distribution of the maximum principle stress can be explained as follows. As the maximum temperature occurs in the slicing kerf as shown in Fig. 13, the expansion of material here is restricted by the surrounding material. The material around the kerf suffers compressive stress exerted by the surrounding material. As a result, the principle around the kerf is not large.

In the slicing process, the temperature in the place behind the kerf decreases rapidly after the wire saw leaves because of the coolant. As the place behind the kerf contacts with the coolant directly, the temperature here decreases faster than

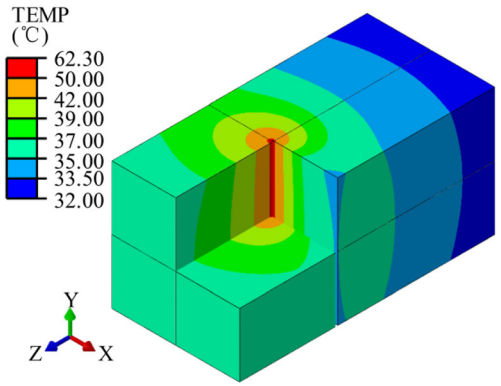

Fig. 10 Distribution of temperature field of the KDP crystal

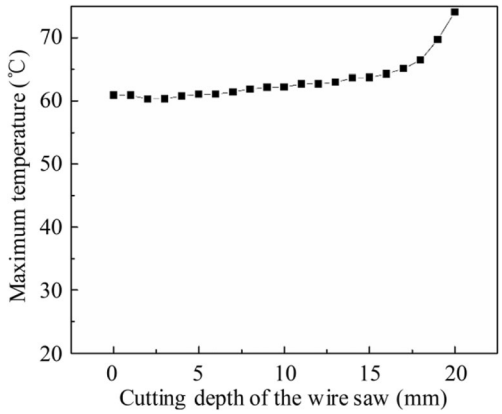

Fig. 11 Variation of maximum temperature with cutting depth

the inner place in the crystal. As the contraction of the material here is limited by the surrounding material, it suffers tensile stress. Then, maximum principle stress in this plane occurs in the place behind the kerf.

We can also notice that the temperature field is not symmetrical in Fig. 13. The kerf is not in the middle of the KDP crystal; the left part is smaller than the right part. As a result, the temperature of the left part is a little higher than the right part.

While the wire saw speed v_s is 1.5 m/s and the feed speed v_w is 0.6 mm/min, variation of maximum principle stress of thermal stress in plane ABCD in the slicing is shown in Fig. 14. It can be seen that, the value of maximum principle stress is about 2 MPa in the beginning of the slicing. It increases with the increasing of the cutting depth and has a peak when the cutting depth is about 5 mm. Then, the maximum principle stress decreases slowly to about 3 MPa till the end of the slicing.

The reason can be explained as follows. The maximum principle stress occurs around the edge in the beginning of the slicing. This is because of the stress concentration of the edge area and contraction of the material. When the cutting depth becomes larger, the maximum principle stress still occurs behind the slicing area and the edge area. At the same time, the effect of contraction of the material becomes larger.

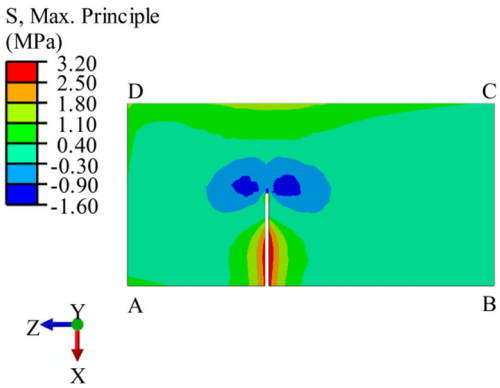

Fig. 12 Maximum principle stress caused by thermal stress in plane ABCD

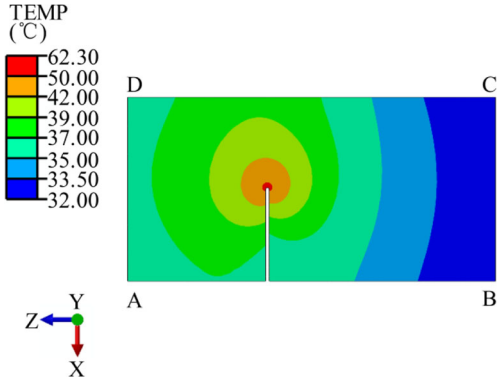

Fig. 13 Temperature field in plane ABCD

As a result, the maximum principle stress increases. When the cutting depth is about 5 mm, the maximum principle stress reaches the largest value of 4.64 MPa. With the increase of the cutting depth, the maximum principle stress does not occur around the edge. Without the stress concentration of the edge, the maximum principle stress decreases. With the increase of the cutting depth, the distance between the palace of maximum principle stress and edge also increases. So the effect of stress concentration of edge to the palace of the maximum principle stress becomes smaller. Then, the maximum principle stress slowly decreases to about 3 MPa and almost remains stable till the end of the slicing.

4.3 Coupling stress in the slicing

While the cutting depth of wire saw is 10 mm, the wire saw speed v_s is 1.5 m/s and the feed speed v_w is 0.6 mm/min, distribution of maximum principle stress of coupling stress in plane ABCD is shown in Fig. 15. It can be noticed that the value of maximum principle stress of coupling stress is almost the same with the thermal stress as shown in Fig. 12.

The comparison of the maximum principle stress in plane ABCD when there is only slicing force, only thermal stress, and coupling stress is shown in Fig. 16. It can be noticed that

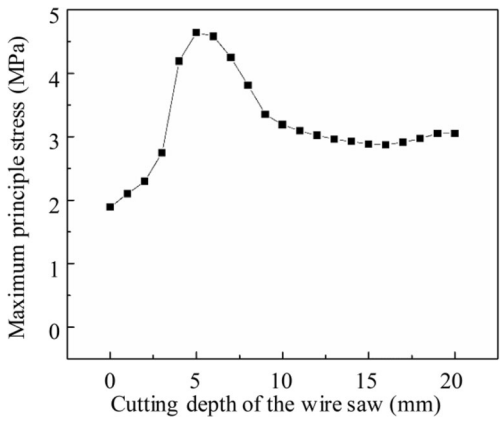

Fig. 14 Variation of maximum principle stress caused by thermal stress in plane ABCD

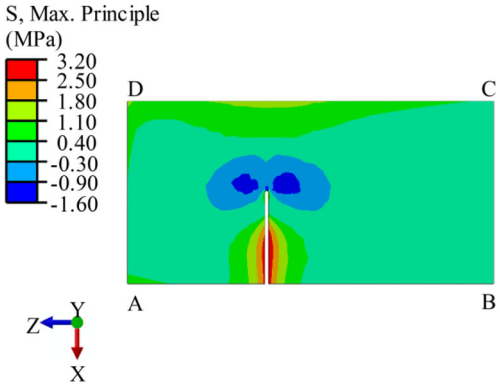

Fig. 15 Maximum principle stress of coupling stress in plane ABCD.

the stress caused by the slicing force is small. The coupling stress is much larger than the stress while only slicing stress is considered. The coupling stress is almost the same with the stress when only thermal stress is considered. It can be concluded that the thermal stress is the major part of the coupling stress in the slicing, as the slicing force and thermal force are two sources of the stress in the slicing. Besides, the coupling stress is close to the real situation. The slicing force cannot be ignored though its value is small.

4.4 Variation of maximum principle stress with slicing parameters

Different groups of slicing parameters are chosen to investigate the influence of slicing parameters to the ingot. The parameters are shown in Table 3. Where $F_{n\theta}$, $F_{t\theta}$, and P_θ are the parameters applied to the FEM model, they are got by Eq. (9).

The variation of maximum principle stress in plane ABCD with the feed speed v_w is shown in Fig. 17. When the wire saw speed v_s is fixed, it can be noticed that the maximum principle stress increases with the increase of feed speed v_w.

The least squares method is used to obtain the function equation between maximum principle stress and feed speed. Equation (11) is then obtained with the correlation coefficient of 1:

$$S_{\max} = 7.735 v_w + 0.001 \tag{11}$$

where $S_{\max}$ is the maximum principle stress in the KDP crystal. From Eq. (11), it can be seen that there is a positive correlation between the maximum principle stress and feed speed. As the tensile strength of the KDP crystal is low, it is easy to crack due to tensile stress. It is considered that when the maximum principle stress is lower than the tensile strength of the KDP crystal, cracks would not occur in the fixed abrasive slicing of the KDP crystal. Then, the critical feed speed at which cracks would not occur can be obtained according to Eq. (11). When v_w is lower than 0.862 mm/min, the maximum principle stress is less than the tensile strength of the KDP crystal. In this condition, cracks may not occur in the slicing.

Variation of maximum principle stress in plane ABCD with the ratio of feed speed to wire saw speed is shown in Fig. 18. It can be seen that there is a positive correlation between the maximum principle stress and the ratio of feed speed to wire saw speed. The maximum principle stress increases with the increase of the ratio of feed speed to wire saw speed.

Table 3 Forces and heat power of different slicing parameters

No.	v_s/(m/s)	v_w/(mm/min)	$F_{n\theta}$/(MPa)	$F_{t\theta}$/(MPa)	P_θ/(10^3N/mms)
1	1.5	0.6	0.51cosθ	0.20cosθ	100cosθ
2	1.5	0.1	0.085cosθ	0.033cosθ	17cosθ
3	1.5	0.2	0.17cosθ	0.067cosθ	33cosθ
4	1.5	3.0	2.55cosθ	1.00cosθ	500cosθ
5	1.5	1.2	1.02cosθ	0.40cosθ	200cosθ
6	0.5	0.6	1.53cosθ	0.60cosθ	100cosθ
7	1.0	0.6	0.77cosθ	0.30cosθ	100cosθ
8	3.0	0.6	0.26cosθ	0.10cosθ	100cosθ
9	7.5	0.6	0.10cosθ	0.040cosθ	100cosθ
10	15.0	0.6	0.051cosθ	0.0020cosθ	100cosθ

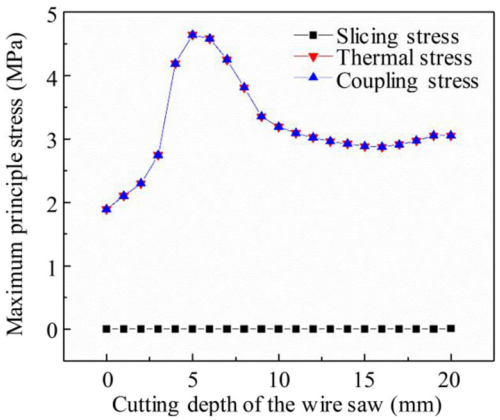

Fig. 16 Comparison of maximum principle stress in plane ABCD

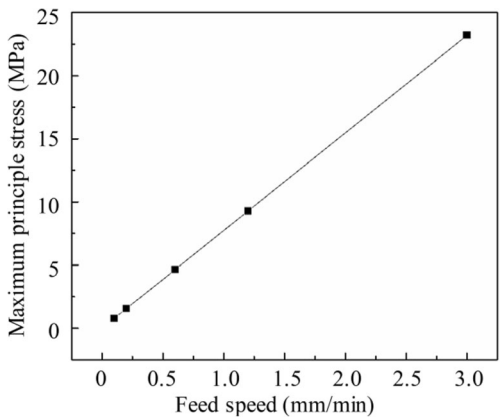

Fig. 17 Variation of maximum principle stress with feed speed

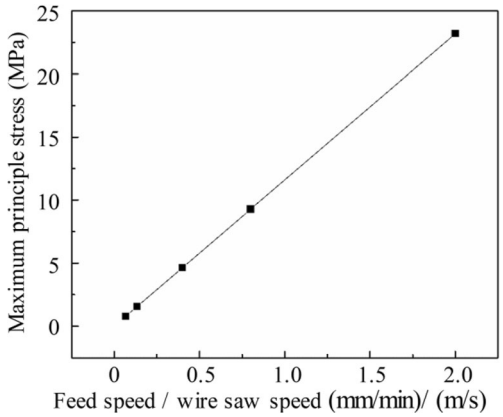

Fig. 18 Variation of maximum principle stress with the ratio of feed speed to wire saw speed

The least squares method is used to obtain the function equation between the maximum principle stress and the ratio of feed speed to wire saw speed. The obtained formula is Eq. (12) with the correlation coefficient of 1:

$$S_{\max} = 11.602(v_w/v_s) - 0.003 \quad (12)$$

It can be seen from Eqs. (11) and (12) that the relationship between the stress and feed speed v_w, as well as the ratio of feed speed and wire saw speed v_w/v_s is almost linear in the study. This can be explained as follows. In Section 2, many assumptions are made such as the abrasives are assumed evenly distributed on the surface of the wire saw and they are in shape of conical. Then, the relationship between the slicing force and feed speed v_w, as well as the ratio of feed speed and wire saw speed v_w/v_s is linear as shown in Eq. (4). In the studies of slicing force for silicon and silicon carbide, when other assumptions are made in the analysis of slicing force of fixed abrasive wire saw, the slicing force and feed speed v_w, as well as the ratio of feed speed and wire saw speed v_w/v_s have a positive correlation [12, 25]. As a result, the relationship between stress and feed speed v_w as well as the ratio of feed speed and wire saw speed v_w/v_s is almost linear in the study.

According to Eq. (12), when the value of v_w/v_s is less than 0.575 (mm/min)/(m/s), the maximum principle stress is lower than the tensile strength of the KDP crystal. In this condition, the KDP crystal would not crack in the slicing.

The results indicated that the ratio of wire saw speed to feed speed 0.575 (mm/min)/(m/s) could be considered as the critical value below which cracks would not occur in fixed abrasive slicing of the KDP crystal.

5 Conclusion

In this study, a finite element model of the KDP crystal in fixed abrasive wire saw slicing is constructed to analyze the maximum principle stress. The conclusions can be summarized as follows:

(1) Temperature field of the KDP crystal in fixed abrasive wire saw slicing is obtained by simulation; the maximum temperature occurs in the kerf area. The maximum temperature almost remains stable when the slicing parameters are fixed.
(2) The maximum principle stress caused by slicing force, thermal stress, and coupling of the slicing force and thermal stress is obtained. The result shows that the stress caused by thermal stress is much larger than that caused by the slicing force. Thermal stress is the main reason of cracking in the KDP crystal slicing with fixed abrasive wire saw.
(3) Variation of maximum principle stress with slicing parameters is obtained; the function is obtained by the least squares method. The ratio of wire saw speed and feed speed 0.575 (mm/min)/(m/s) is the critical value below which cracks would not occur in fixed abrasive slicing of the KDP crystal.

Acknowledgements This work is supported by the National Natural Science Foundation of China (51775317) and the Key Research and Development Program of Shandong Province (2017GGX30142).

References

1. Chen M, Pang Q, Wang J, Cheng K (2008) Analysis of 3D microtopography in machined KDP crystal surfaces based on fractal and wavelet methods. Int J Mach Tool Manu 48(7–8):905–913
2. He Z, Huang H, Yin F, Xu X (2017) Development of a brazed diamond wire for slicing single-crystal SiC ingots. Int J Adv Manuf Tech 91(1–4):189–199
3. Pritula IM, Bezkrovnaya ON, Lopin AV, Kolybaeva MI, Puzikov VM, Zubatyuk RI, Shishkin OV, Gayvoronsky VY (2013) Optical properties of KDP crystals doped with pyrenetetrasulfonic acid salt. J Phys Chem Solids 74(3):452–456
4. Chen N, Chen M, Guo Y, Wang X (2015) Effect of cutting parameters on surface quality in ductile cutting of KDP crystal using self-developed micro PCD ball end mill. Int J Adv Manuf Tech 78(1–4): 221–229
5. Zong WJ, Li ZQ, Zhang L, Liang YC, Sun T, An CH, Zhang JF, Zhou L, Wang J (2013) Finite element simulation of diamond tool geometries affecting the 3D surface topography in fly cutting of KDP crystals. Int J Adv Manuf Tech 68(9–12):1927–1936
6. Chen D, Chen J, Wang B (2016) A hybrid method for crackless and high-efficiency ultraprecision chamfering of KDP crystal. Int J Adv Manuf Tech 87(1–4):293–302
7. Wang X, Gao H, Chen Y, Guo D (2016) A water dissolution method for removing micro-waviness caused by SPDT process on KDP crystals. Int J Adv Manuf Tech 85(5–8):1347–1360
8. Deng L, Duan J, Zeng X, Yang H, Huang S (2013) A study on dual laser beam separation technology of KDP crystal. Int J Mach Tool Manu 72:1–10
9. Deng L, Yang H, Zeng X, Wu B, Liu P, Wang X, Duan J (2015) Study on mechanics and key technologies of laser nondestructive mirror-separation for KDP crystal. Int J Mach Tool Manu 94:26–36

10. Wang Q, Cong W, Pei ZJ, Gao H, Kang R (2009) Rotary ultrasonic machining of potassium dihydrogen phosphate (KDP) crystal: an experimental investigation on surface roughness. J Manuf Process 11(2):66–73
11. Wu H (2016) Wire sawing technology: a state-of-the-art review. Precis Eng 43:1–9
12. Wang P, Ge P, Gao Y, Bi W (2017) Prediction of sawing force for single-crystal silicon carbide with fixed abrasive diamond wire saw. Mat Sci Semicon Proc 63:25–32
13. Huang H, Zhang Y, Xu X (2015) Experimental investigation on the machining characteristics of single-crystal SiC sawing with the fixed diamond wire. Int J Adv Manuf Tech 81(5–8):955–965
14. Gao Y, Ge P, Liu T (2016) Experiment study on electroplated diamond wire saw slicing single-crystal silicon. Mat Sci Semicon Proc 56:106–114
15. Clark WI, Shih AJ, Lemaster RL, McSpadden SB (2003) Fixed abrasive diamond wire machining—part II: experiment design and results. Int J Mach Tool Manu 43(5):533–542
16. Ge M, Bi W, Ge P, Bi Y (2016) Experimental research on KDP crystal slicing with resin bonded diamond abrasive wire saw. Int J Adv Manuf Tech 87(5–8):1671–1676
17. Clark WI, Shih AJ, Hardin CW, Lemaster RL, McSpadden SB (2003) Fixed abrasive diamond wire machining—part I: process monitoring and wire tension force. Int J Mach Tool Manu 43(5): 523–532
18. Chung C, Tsay GD, Tsai MH (2014) Distribution of diamond grains in fixed abrasive wire sawing process. Int J Adv Manuf Tech 73(9–12):1485–1494
19. Zhang Q, Zhang N, Wang S, Liu D (2009) Analysis of the size effect of crack generation in the large-scale KDP crystals during its growth. J Funct Mater 40(9):1584–1590
20. Zhang N, Zhang Q, Wang S, Sun Y (2011) Analysis of mechanical effects for the cracks in large-scale KDP crystals during getting out from crystallizers with numerical simulation method. J Funct Mater 42(12):2133–2136
21. Ge M, Gao Y, Ge P, Jiao Y, Bi W (2017) A finite element analysis of sawing stress in fixed-abrasive wire saw slicing KDP crystal. Int J Adv Manuf Tech 91(5–8):2049–2057
22. Bhagavat S, Kao I (2008) A finite element analysis of temperature variation in silicon wafers during wiresaw slicing. Int J Mach Tool Manu 48(1):95–106
23. Johnsen L, Olsen JE, Bergstrom T, Gastinger K (2012) Heat transfer during multiwire sawing of silicon wafers. J Therm Sci Eng Appl 4(3):031006
24. Jiao Y, Ge P, Gao Y, Bi W (2014) Analysis of temperature and thermal stress distribution on KDP crystal wire saw slicing. Adv Mater Res 1027:28–31
25. Liu T, Ge P, Gao Y, Bi W (2017) Depth of cut for single abrasive and cutting force in resin bonded diamond wire sawing. Int J Adv Manuf Tech 88(5–8):1763–1773
26. Meng JF (2006) Research on machined technology and machined quality of endless electroplated diamond wire saw. Dissertation, University of Shandong
27. Zhang QY, Liu DJ, Wang SL, Zhang N, Mou XM, Sun Y (2009) Mechanical parameters test and analysis for KDP crystal. J Syn Cryst 38(6):1313–1319
28. Liu L, Wang SL, Liu GX, Wang DL, Li WD, Ding JX (2015) Research on thermal expansion coefficient of large-aperture KDP/DKDP crystals. J Syn Cryst 44(6):1443–1447
29. Nikogosyan DN (2005) Nonlinear optical crystals: a complete survey. Springer, New York
30. Fang T, Lambropoulos JC (2002) Microhardness and indentation fracture of potassium dihydrogen phosphate (KDP). J Am Ceram Soc 85(1):174–178

Publisher's Note